Accepted Manuscript

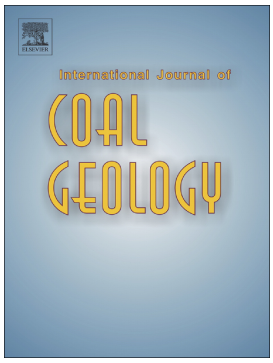

Characterisation of creep in coal and its impact on permeability: An experimental study

Nima N. Danesh, Zhongwei Chen, Luke D. Connell, Mehmet S. Kizil, Zhejun Pan, Saiied M. Aminossadati

PII: S0166-5162(16)30647-4
DOI: doi: 10.1016/j.coal.2017.03.003
Reference: COGEL 2801

To appear in: *International Journal of Coal Geology*

Received date: 21 October 2016
Revised date: 3 February 2017
Accepted date: 3 March 2017

Please cite this article as: Nima N. Danesh, Zhongwei Chen, Luke D. Connell, Mehmet S. Kizil, Zhejun Pan, Saiied M. Aminossadati , Characterisation of creep in coal and its impact on permeability: An experimental study. The address for the corresponding author was captured as affiliation for all authors. Please check if appropriate. Cogel(2017), doi: 10.1016/j.coal.2017.03.003

Characterisation of Creep in Coal and its Impact on Permeability: An Experimental Study

Nima N. Danesh[1], Zhongwei Chen[1,*], Luke D. Connell[2], Mehmet S. Kizil[1], Zhejun Pan[2], Saiied M. Aminossadati[1]

[1] *School of Mechanical and Mining Engineering, the University of Queensland, QLD 4072, Australia*
[2] *CSIRO Energy Flagship, Clayton South 3169, Australia*
** Corresponding author's email address: zhongwei.chen@uq.edu.au*

ABSTRACT: Creep is a time-dependent deformation that affects coal permeability and should be considered in the prediction of Coalbed Methane (CBM) production. This study experimentally characterises and quantifies the impact of creep on coal permeability. The experiments were conducted on a bituminous coal sample, excavated from Bowen Basin, Australia, using a triaxial gas rig equipped with strain and displacement transducers. Two different types of gasses (helium and methane) were injected into the sample under various stress and pore pressure conditions. It was found that for the experiments with helium, creep caused permanent partial closure of cleats and pathways under constant effective stress, and hence a reduction in permeability. Under hydrostatic stress only, a Residual Deformation Ratio (*RDR*) of 14.1% and a Permeability Loss Ratio (*PLR*) of 71% were found following the removal of the axial load. This can be due to the damage to coal microstructure along with closure of cleats. For the experiments with methane, coal experienced an instantaneous elastic deformation, at the onset of pore pressure depletion, followed by consolidation and matrix shrinkage. Then, creep occurred when gas desorption ceased. A total permeability loss of 26% was achieved due to an increase of 1.91 MPa in effective stress caused by gas desorption. In addition, the model previously developed by authors was validated against the experimental permeability data. A good agreement was found between the model-predicted permeability data and the experimental permeability data, particularly for higher pore pressure ranges.

Keywords: Coal permeability; creep; consolidation; triaxial test; gas desorption

Nomenclature

A, B, C = experimental coefficients, dimensionless
c_f = fracture compressibility, Pa^{-1}
E_e = Young's modulus of elasticity, Pa
$E_{e,i}$ = Young's modulus of elasticity in i direction ($i = x, y, z$), Pa
$E_{e,j}$ = Young's modulus of elasticity in j direction ($j = x, y, z$), Pa
E_{ve} = Young's modulus of visco-elasticity, Pa
$E_{ve,i}$ = Young's modulus of visco-elasticity in i direction ($i = x, y, z$), Pa
k = permeability, Darcy
k_0 = initial permeability, Darcy
p = pore pressure, Pa
p_0 = initial pore pressure, Pa
P_d = downstream pressure, Pa
P_L = Langmuir pressure constant, Pa
P_u = upstream pressure, Pa
PLR = porosity loss ratio, dimensionless
Q = flow rate, m^3/s
RDR = residual deformation ratio, dimensionless
t = time, hr
t_f = failure time, hr
t_y = yield time, hr
V_L = Langmuir volume constant, m^3/kg

Greek letters

α_i = thermal coefficient in i direction ($i = x, y, z$), °C^{-1}

$\Delta\varepsilon_T$ = thermal strain increment, dimensionless

$\Delta\varepsilon_{T,i}$ = directional thermal strain increment ($i = x, y, z$), dimensionless

$\Delta\varepsilon^{s,axi}$ = axial shrinkage strain increment, dimensionless

$\Delta\varepsilon_{max}^{s,axi}$ = maximum axial shrinkage strain increment, dimensionless

$\Delta\varepsilon_i$ = directional total strain ($i = x, y, z$), dimensionless

$\Delta\varepsilon_i^s$ = shrinkage strain increment in i direction ($i = x, y, z$), dimensionless

$\Delta\varepsilon_{axi}^{con,s}$ = axial consolidation and shrinkage strains

$\Delta\varepsilon_{axi}$ = total axial strain increment, dimensionless

$\Delta\varepsilon_{e,axi}$ = axial elastic strain increment, dimensionless

$\Delta\varepsilon_{ve,axi}$ = axial visco-elastic strain increment, dimensionless

$\Delta\varepsilon_{vp\text{-}lt,axi}$ = visco-plastic deformation in axial direction, if long-term strength exceeded

$\Delta\varepsilon_{vp\text{-}st,axi}$ = visco-plastic deformation in axial direction, if short-term strength exceeded

$\Delta\sigma_{eff,i}$ = effective stress increment in i direction ($i = x, y, z$), Pa

$\Delta\sigma_i$ = stress increment in i direction ($i = x, y, z$), Pa

$\Delta\sigma_j$ = stress increment in j direction ($j = x, y, z$), Pa

ΔT = temperature increment, °C

ε = total strain, dimensionless

ε_e = elastic strain, dimensionless

ε_L = parameter of Langmuir curve, dimensionless

$\varepsilon_{max,axi}$ = maximum axial deformation, dimensionless

ε_p = plastic or residual deformation, dimensionless

ε_{ve} = visco-elastic strain, dimensionless

ε_{vp} = visco-plastic strain, dimensionless

η_i = viscosity coefficient in i direction ($i = x, y, z$), Pa.s

η_j = viscosity coefficient in j direction ($j = x, y, z$), Pa.s

η_{ve} = viscosity coefficient of visco-elastic media, Pa.s

$\eta_{ve,i}$ = viscosity coefficient of visco-elastic media in i direction ($i = x, y, z$), Pa.s

η_{vp} = viscosity coefficient of visco-plastic media, Pa.s

μ = gas viscosity, Pa.s

υ = Poisson's ratio, dimensionless

υ_{ji} = component of the Poisson's ratio tensor ($i, j = x, y, z; i \neq j$), dimensionless

σ = stress, Pa

σ_a = axial stress, Pa

σ_h^e = horizontal effective stress, Pa

σ_{h0}^e = initial horizontal effective stress, Pa

σ_{ls} = long-term strength, Pa

σ_r = radial stress, Pa

σ_{ss} = short-term strength, Pa

1. Introduction

Coal permeability is a critical parameter for the prediction and evaluation of Coalbed Methane (CBM) production. Coal is a dual-porosity medium composed of cleats and matrices, which are the main conduit for gas migration and storage site, respectively. The change of coal permeability results from variation of effective stress and shrinkage and swelling of coal matrix owing to desorption and sorption of the gases in the reservoir. Matrix shrinkage and cleat compression mechanisms have inverse effects on permeability during CBM production. Whereas matrix shrinkage leads to dilation of coal cleat and increase in permeability, cleat compression results in decrease in permeability. The effects of the two mechanisms on coal permeability have been extensively studied (Levine, 1996; Palmer and Mansoori, 1996, 1998; Seidle and Huitt, 1995; Shi and Durucan, 2004).

Alteration in porosity due to deformation of cleat-matrix assemblage leads to change of permeability. Deformation in coal can occur much faster due to being much softer than adjacent rocks (roof and floor rocks) (Brantut et al., 2013; Kaiser and Morgenstein, 1981). The relative softness of coal is due to large macromolecular organic networks in coal that do not possess strong bonds (Espinoza et al., 2016). Coal deformation process occurs at very slow rates during coalification and formation of overlying sedimentary rocks over geologic time scales. However, the deformation process (elastic and/or inelastic) may accelerate due to increasing effective stress during extraction of fluids in the reservoir (Schatz and Carroll, 1981). The impact of elastic deformation on coal permeability has been considered by some researchers (Liu and Rutqvist, 2010; Pan and Connell, 2011; Shi and Durucan, 2004). Nevertheless, investigations on the effect of inelastic deformation on coal permeability have not been carried out rigorously. Inelastic deformation of coal may occur during CBM production and well shut-in at static pore pressure. Compaction of coal reservoir occurs due to pressure depletion under uniaxial strain condition (the reservoir is confined laterally), which causes reduction in permeability and hence production rate (Wang et al., 2012). The mechanically induced compaction of coal due to increased effective stress is generally called primary consolidation, which is an inelastic deformation. When effective stress is constant, the compaction is known as secondary consolidation or creep, which is also an inelastic deformation (Barden, 1968; Bjørlykke et al., 2010). However, it is sometimes difficult to differentiate between genuine creep and consolidation effects (Fjær et al., 2008).

Creep is a mechanical and/or chemical process that is initiated by microstructure deterioration or restructuring of rocks. It is affected by parameters such as temperature, stress, and time. Creep can occur through four mechanisms namely: (1) Cataclasis: a delayed deterioration of microstructure that its dependency on time is relatively negligible and also generates a finite stress-dependent deformation (Fabre and Pellet, 2006; Frayne et al., 1990); (2) Pressure solution: solubility of the solids immersed in liquids change with stress (Yost and Aronson, 1987), or in other words, stress induces dissolution-precipitation. This type of creep may be dominant when water-gas two phase flow exists in coal reservoir; (3) Granular creep or particulate sliding: the imposition of grains rearrangement by frictional sliding as well as pressure solution in order to accommodate grain shape alteration throughout compaction process (Frayne et al., 1990); and (4) Adsorption-diffusion: a temporary compaction deformation induced by adsorption or diffusion which is different from that of permanent deformation of solid phase (Hol et al., 2013; Sone and Zoback, 2010). The dominant creep mechanism is determined by material properties such as moisture content, grain size, and strength as well as in situ conditions such as stress and strain rates (Frayne et al., 1990). Considering single-phase flow in coal, the dominant creep mechanisms are cataclasis and particulate sliding. In cataclastic flow regime, permeability and porosity are affected by the development of microstructure during

compressive cataclastic failure (Zhu and Wong, 1997). Development of compaction is influenced by initial stress state and the stress path in the reservoir during drainage (Settari, 2002).

The impact of mechanical properties and rank on coal deformation and permeability has been extensively studied. Uniaxial compressive strength and Young's modulus increase with coal rank. This is due to less microporous structure of higher rank coal (Pan et al., 2013). Also, studies show higher permeability with pore pressure depletion for the coal with higher lateral Young's modulus (parallel to bedding) (Danesh et al., 2016; Pan and Connell, 2011). Higher rank coals such as anthracite do not creep and generally break explosively in uniaxial compression tests (Pomeroy, 1956). This is because coal matrix and cleat systems are generally stiffer (or denser) in higher rank coals, during the loading process under equal conditions, so that the matrix and cleat systems accommodate less creep deformation compared to lower rank coals. Hence, permeability change for higher rank coals is expected to be less.

Triaxial compression tests have been conducted for simulation of in-situ conditions for coal in order to measure coal geomechanical properties. In such tests, axial and hydrostatic stresses are applied to the coal core that is saturated with a specific gas (e.g. CH_4, CO_2, N_2). Some studies have been carried out on coal characteristics under triaxial compression (Hobbs, 1964; Lin, 2010; Pan et al., 2010) as well as when high pressure gas is involved (Alexeev et al., 2012; Ujihira et al., 1985). In addition, creep behaviour of coal saturated with gas has been studied (Wang et al., 2011; Yang and Zoback, 2011; Yin et al., 2009; Yin et al., 2008; Zhu et al., 2011). Different types of gases have diverse adsorption capacity and consequently show dissimilar creep behaviours. The more the adsorption capacity of the gas is, the softer the coal becomes due to greater degree of coal matrix swelling. Yang and Zoback (2011) studied the effect of gas type on visco-plastic behaviour. They utilised He, N_2, CH_4, and CO_2 in their experiments to examine the impact of adsorption of various gases on the mechanical and flow properties of coal. Their results show that the gas with higher adsorption capacity induces greater matrix swelling and therefore weakening of the coal mass that causes more creep in the coal than the gas with lower adsorption capacity. More recently, Danesh et al. (2016) developed a new stress-strain model to reflect the impact of inelastic deformation on coal permeability, and compared the change in gas production with and without inelastic deformation.

As aforementioned, creep behaviour of the coal saturated with gas has been widely studied. However, experimental studies that explicitly consider the influence of consolidation and creep (i.e. primary consolidation and secondary consolidation) on permeability of the coal saturated with different gasses under varying stress conditions have yet to be conducted. In this study, a bituminous coal sample saturated with the gas (helium for the first test and methane for the second test), which was accommodated in a triaxial rig was used. For the case of helium, creep was induced by applying an axial load to the coal sample after the sample has reached equilibrium under hydrostatic stress. For the case of methane, gas production process was simulated by pore pressure depletion due to gas desorption from the same sample under constant hydrostatic and axial stress conditions. Permeability measurements were performed before and after the change in the effective stress.

2. Mechanical model

2.1. Creep strain in coal

Fig. 1 shows a typical creep curve of coal under deviatoric stress condition. It consists of three stages: (1) primary or decelerating creep; (2) secondary or steady-state creep; and (3) tertiary or accelerating

creep. Strain rate decreases with time in primary creep; then, it becomes zero in steady-state creep; and finally, it increases with time in tertiary creep.

Creep is normally modelled through exponential (Bai et al., 2012; Brantut et al., 2013; Li et al., 2011; Li et al., 2013; Nishihara, 1952, 1957; Yin et al., 2009; Yin et al., 2008) and power functions (Cruden et al., 1987; Singh, 1975; Wang et al., 2011). Classical Nishihara model, as shown in Fig. 2, is comprised of the Hooke body, the visco-elastic body, and the visco-plastic body.

The total strain of Nishihara model (Nishihara, 1952) can be written as:

$$\varepsilon = \varepsilon_e + \varepsilon_{ve} + \varepsilon_{vp} \tag{1}$$

where, ε_e is the elastic strain, ε_{ve} is the visco-elastic strain, and ε_{vp} is the visco-plastic strain.

Eq. 1 can be extended depending on the stress conditions as follows (Jiang et al., 2012; Yin et al., 2009; Yin et al., 2008):

$$\varepsilon = \frac{\sigma}{E_e} + \frac{\sigma}{E_{ve}}\left[1 - \exp\left(-\frac{E_{ve}}{\eta_{ve}}t\right)\right], \quad \text{if } \sigma < \sigma_{ss} < \sigma_{ls} \text{ and } 0 < t < t_y \tag{2}$$

$$\varepsilon = \frac{\sigma}{E_e} + \frac{\sigma}{E_{ve}}\left[1 - \exp\left(-\frac{E_{ve}}{\eta_{ve}}t\right)\right] + \frac{\sigma - \sigma_{ss}}{\eta_{vp}}t, \quad \text{if } \sigma_{ss} \le \sigma < \sigma_{ls} \text{ and } 0 < t < t_y \tag{3}$$

$$\varepsilon = \frac{\sigma}{E_e} + \frac{\sigma}{E_{ve}}\left[1 - \exp\left(-\frac{E_{ve}}{\eta_{ve}}t\right)\right] + \frac{(\sigma - \sigma_{ls})}{C\eta_{vp}}\left(\frac{A}{3}t^3 - \frac{B}{2}t^2 + Ct\right), \quad \text{if } \sigma \ge \sigma_{ls} \text{ and } 0 < t < t_f \tag{4}$$

On the right side of Eqs. 2-4, the first and second terms represent elastic and visco-elastic strains, respectively. The third term in Eq. 3 denotes visco-plastic strain when stress exceeds short-term strength (σ_{ss}). The third term in Eq. 4 denotes visco-plastic strain when stress exceeds long-term strength (σ_{ls}). Eq. 2 is valid when the stress applied to coal is less than short-term strength and long-term strength. Eq. 3 is valid for the case that the stress exerted to coal is larger than short-term strength and smaller than long-term strength. If the stress applied to coal exceeds long-term strength, creep process accelerates in tertiary creep until coal fails. Eq. 4 can be used for modelling creep in the latter case.

2.2. Linear stress-strain relation for anisotropic coal

Jaeger and Cook (1969) suggested a constitutive equation for anisotropic poroelastic media with orthorhombic symmetry (3D). The stress-strain relation for the coal reservoir considering anisotropic matrix swelling/shrinkage strain and thermal expansion/contraction strain can be written as:

$$\Delta\varepsilon_i = \Delta\varepsilon_{e,i} + \Delta\varepsilon_i^s + \Delta\varepsilon_{T,i}, \qquad i = x, y, z \tag{5}$$

where, $\Delta\varepsilon_i$ is the directional total strain, $\Delta\varepsilon_{e,i}$ is the directional elastic strain obeying Hooke's law, $\Delta\varepsilon_i^s$ is the swelling/shrinkage strain, and $\Delta\varepsilon_{T,i}$ denotes the directional thermal expansion/contraction strain.

Extending Eq. 5, the common stress-strain relationship for anisotropic poroelastic media with orthorhombic symmetry was suggested by Jaeger et al. (2007) as follows:

$$\Delta\varepsilon_i = \frac{\Delta\sigma_i}{E_{e,i}} - \sum_{j=x,\,j\neq i}^{z}\left[\upsilon_{ji}\frac{\Delta\sigma_j}{E_{e,j}}\right] + \Delta\varepsilon_i^s + \alpha_i\Delta T\,, \qquad i = x, y, z \tag{6}$$

2.3. Non-linear stress-strain relation for anisotropic coal

A non-linear stress-strain relation for anisotropic poroelastic and visco-elastic continua was suggested by (Danesh et al., 2016) through extending the constitutive equation of Jaeger and Cook (1969) as follows:

$$\Delta\varepsilon_i = \Delta\varepsilon_{e,i} + \Delta\varepsilon_{ve,i} + \Delta\varepsilon_i^s + \Delta\varepsilon_{T,i}\,, \qquad i = x, y, z \tag{7}$$

where,

$$\Delta\varepsilon_{e,i} = \frac{\Delta\sigma_i}{E_{e,i}} - \sum_{j=x,\,j\neq i}^{z}\left[\upsilon_{ji}\frac{\Delta\sigma_j}{E_{e,j}}\right] \tag{8}$$

$\Delta\varepsilon_{ve,i}$ is the directional visco-elastic strain and is derived from Nishihara model (Nishihara, 1952, 1957), which can be written as follows:

$$\Delta\varepsilon_{ve,i} = \frac{\Delta\sigma_i}{E_{ve,i}}\left[1-\exp\left(\frac{-E_{ve,i}}{\eta_i}t\right)\right] - \sum_{j=x,\,j\neq i}^{z}\left[\upsilon_{ji}\frac{\Delta\sigma_j}{E_{ve,j}}\left[1-\exp\left(\frac{-E_{ve,j}}{\eta_j}t\right)\right]\right], \qquad i = x, y, z \tag{9}$$

Inserting Eqs. 8 and 9 in Eq. 7 yields:

$$\Delta\varepsilon_i = \frac{\Delta\sigma_i}{E_{e,i}} + \frac{\Delta\sigma_i}{E_{ve,i}}\left[1-\exp\left(\frac{-E_{ve,i}}{\eta_i}t\right)\right] - \sum_{j=x,\,j\neq i}^{z}\left[\upsilon_{ji}\left[\frac{\Delta\sigma_j}{E_{e,j}} + \frac{\Delta\sigma_j}{E_{ve,j}}\left[1-\exp\left(\frac{-E_{ve,j}}{\eta_j}t\right)\right]\right]\right] + \Delta\varepsilon_i^s + \alpha_i\Delta T\,, \quad i = x, y, z \tag{10}$$

Eq. 10 will be used as a regression equation to obtain the values of unknown parameters and strain components by fitting the experimental data. The parameter values will then be implemented into a permeability model, which will be validated against the experimental permeability data.

3. Experimental measurement of creep

3.1. Experimental set-up

A triaxial gas rig was used to study the impact of creep on coal permeability (Fig. 3). The rig was equipped with two axial displacement transducers and two radial strain gauges used for measuring axial displacements and radial strains. It was also capable of applying hydrostatic and axial loads separately. The two radial strain gauges were installed on the sample perpendicularly. The sample used for the experiments was a high-volatile bituminous coal excavated from Bowen Basin, Australia (see Fig. 4). The sample was cored parallel to the bedding plane and face cleats were parallel to the axis of the sample. The diameter and length of the coal sample were 6.1 cm and 9.5 cm, respectively. The sample was dried in a heated vacuum oven at 50°C and its weight was measured before installation. A membrane was also placed around the sample to isolate the sample from the confining fluid. Uneven surface of the sample was smoothened using plaster to avoid the build-up of localised stress concentration and gas leakage through the membrane. Once the sample was installed in the gas cell, a series of load cycles were applied to consolidate the sample and provide in-situ stress

conditions. When axial load was applied, total axial stress was equal to the summation of hydrostatic stress and axial stress. This means the total axial stress was always higher than radial stress ($\sigma_a > \sigma_r$). The rig cell and other parts were accommodated in a cabinet to provide isothermal condition throughout the tests.

3.2. Results and discussion

3.2.1. Influence of constant effective stress using helium

This section presents the results of a triaxial test conducted to study the impact of constant effective stress on creep behaviour and permeability of coal saturated with helium. The aim of this test was to perform strain and permeability measurements to study the effect of creep on coal permeability. In this test, the hydrostatic stress of 1.5 MPa was initially applied to the sample. Then, helium was injected into the sample at 0.5 MPa. When strain rate zeroed under constant hydrostatic stress, an axial load of 3 MPa was applied to the coal sample (total axial load of 4.5 MPa), as shown in Fig. 5. The stresses and pore pressure were maintained constant for 8 days and then the axial stress was removed to unload the sample back to hydrostatic condition. Since the gas was not drained from the sample during axial loading and unloading, effective stress was constant throughout the deformation process. It should be noted that the test was not extended for a longer period due to experimental time constraints.

Fig. 6 presents (a) experimental axial creep data and its components under hydrostatic loading and hydrostatic and axial loading conditions, and (b) the rheological model (combination of simple Prandtl and Kelvin-Voigt models) corresponding to the strain data. Applying axial loading, when zero strain rate was achieved in the sample under hydrostatic loading, resulted in an instantaneous elastic deformation under constant effective stress. This behaviour can primarily be attributed to closure of butt cleats and axial compaction of matrix. The compaction of matrix is likely to be due to the softening effect exerted by diffusion of helium from coal cleat into the matrix during injection. The primary creep occurred in a relatively short period and zero strain rate was achieved in the secondary creep. The sample underwent visco-elastic deformation in primary and secondary creep, which comprises smaller portion of the total axial creep compared to elasto-plastic deformation. This behaviour can be associated with time-dependent viscous deformation of coal cleats and matrix. Tertiary creep did not occur in the sample under the test condition. Once the axial load was removed, the sample underwent instantaneous or elastic strain recovery and visco-elastic strain recovery (time-dependent relaxation) under hydrostatic stress only. In this test, the short-term strength of the coal was not exceeded and hence the sample did not experience visco-plastic deformation in the secondary creep stage. The maximum axial deformation of the sample was 0.24%. A residual deformation or plastic deformation of 0.034% was achieved within two and a half days after unloading the sample. This irrecoverable deformation can be linked to the damage to coal microstructure reflected as granular creep and cataclasis. To better understand the effect of creep on coal under axial loading and unloading conditions, the Residual Deformation Ratio (*RDR*) can be defined as follows:

$$RDR\ (\%) = \frac{\varepsilon_p}{\varepsilon_{\max,\mathrm{axi}}} \times 100\% \tag{11}$$

where, ε_p is the plastic or residual deformation after removal of axial load and $\varepsilon_{\max,\mathrm{axi}}$ denotes maximum axial deformation achieved during creep. According to the definition, the *RDR* value for the test using helium gas is 14.1%.

Fig. 7 shows the experimental results of permeability as well as axial strain of the coal sample against time. It also shows the standard error of the mean for the permeability measurements. The permeability of the coal sample can be calculated through the following equation:

$$k = \frac{Q\mu L}{A(P_a - P_b)} \tag{12}$$

where, Q is the measured gas flow rate downstream, μ is the gas viscosity, A is the cross-sectional area of the sample, L is the length of the sample, and P_a and P_b are the pressures across the cross-sectional area of the sample (Fig. 4).

Permeability was measured at 4 stages of: (1) just before applying axial load and under hydrostatic stress only (k_1); (2) after applying axial load and in elastic deformation zone (before initiation of primary creep) (k_2); (3) before unloading in secondary creep (k_3); and (4) after removal of axial load and during visco-elastic strain recovery (k_4) (Figs. 5 and 7). The results show a significant drop of 8.6% (i.e. $((k_2 - k_1)/k_1)\times 100\%$) in permeability due to elastic deformation. The decrease in permeability due to visco-elastic creep is only 0.1% (i.e. $((k_3 - k_2)/k_2)\times 100\%$). When the axial load was removed, permeability increased by 2.8% (i.e. $((k_4 - k_3)/k_3)\times 100\%$) due to elastic and viscoelastic strain recovery. Finally, permeability loss of 6.2% (i.e. $((k_4 - k_1)/k_1)\times 100\%$) caused by plastic deformation was achieved in this test.

Based on the definition of *RDR*, the Permeability Loss Ratio (*PLR*) owing to irrecoverable strain can be calculated through the following equation:

$$PLR\ (\%) = \frac{k_4 - k_1}{k_3 - k_1}\times 100\% \tag{13}$$

A *PLR* of 71% was achieved after removal of the axial load (under hydrostatic stress only). The permeability loss can be linked to permanent partial closure of coal butt cleats and radial expansion of matrix that contributes to permanent partial closure of face cleats as the major conduits for gas flow along the sample.

3.2.2. Influence of increased effective stress using methane

Another set of tests were carried out to investigate the effect of creep (secondary consolidation) on coal permeability after termination of methane gas desorption when pore pressure equilibrium has reached. In this test, the coal sample was initially saturated with methane gas and then, the pore pressure was reduced in three steps to simulate gas production while keeping the hydrostatic and axial stresses constant. Desorption was carried out from both ends of the sample and the differential pressure between upstream and downstream of the core (PT-5 and PT-6 shown in Fig. 3) was maintained constant throughout the process. The pore pressure reduced gradually from 2.48 MPa to 1.49 MPa and then to 1 MPa and finally to 0.57 MPa, shown in Fig. 8. Effective stress increments obtained for each pore pressure change in three steps varied from 0.99 MPa to 1.48 MPa and 1.91 MPa.

Fig. 9 shows the axial strain against time. The deformation process follows the typical creep curve (Fig. 1) and terminates in steady-state creep. The elastic strain of the sample occurs at the onset of pore pressure depletion, which is mainly attributed to closure of coal cleats. The strain rate decelerates due to consolidation and matrix shrinkage and then, it approximately becomes constant reflecting steady state deformation. It is likely that time-dependent closure of coal cleats, particulate sliding, and

cataclasis exert the creep behaviour at pore pressure equilibrium, under deviatoric stress-controlled condition.

Fig. 10 shows the change in volume of desorbed gas from the sample with time for three effective stress increments. The results reveal that the time required for the gas volume to reach equilibrium state decreases with increasing total effective stress increment at each step. For instance, it took approximately 100 hrs for the gas desorption volume to reach steady state for the total effective stress increment of 0.99 MPa in the first step. However, equilibrium was reached longer at approximately 150 hrs for the case of 1.48 MPa in the second step and 320 hrs for the case of 1.91 MPa in the third step. This was due to compaction of coal microstructure and reduction in cleat aperture, which resulted in slower gas flow through the cleats and pathways.

Once the axial load was removed, the sample deformation partially recovered instantaneously followed by visco-elastic relaxation under hydrostatic stress condition. The instantaneous elastic strain recovery is mainly attributed to partial opening of the cleats and expansion of matrix due to the cushioning effect induced by methane. The visco-elastic strain recovery can also be due to time-dependent opening of the cleats and expansion of matrix. Plastic deformation as irrecoverable strain in the sample, after removal of axial load, may be associated with the damage to coal microstructure (particulate sliding and cataclasis).

Permeability measurements were performed at different stages of the test as shown in Fig. 9 in red marks. Permeability was measured at 5 stages of: (1) just before start of pore pressure depletion when all stresses and pore pressure have equilibrated (k_1); (2) before the second step change in pore pressure when effective stress was constant (k_2); (3) before the third step change when effective stress was constant (k_3); (4) before removal of axial load (before the fourth step) under constant effective stress (k_4); and (5) after removal of axial load (k_5) (Figs. 8 and 9). Permeability values were used for calculations and validation of the permeability model developed by Danesh et al. (2016).

Fig. 11 shows permeability change with (a) pore gas pressure and (b) time. In this test, the permeability dropped at each step change in effective stress from 5.6 mD to 4.66 mD, 4.38 mD, and 4.14 mD. No permeability rebound was observed due to stress-controlled condition. The total deformation, including consolidation, matrix shrinkage, and creep induced by an increase of 1.91 MPa in effective stress during desorption caused 26% drop in coal permeability (from 5.6 mD to 4.14 mD) within the studied time frame. After removal of axial load, permeability increased from 4.14 mD to 4.22 mD due to partial recovery of elastic and inelastic deformation.

The measured deformation is comprised of elastic strain, matrix shrinkage strain and time-dependent strains of consolidation and creep. In order to quantify the contribution of each component to coal permeability change, it is critical that their values are obtained. In the following, an extended stress-strain model is employed to determine the strain value of each component by fitting the experimental strain data. Total axial strain for the coal saturated with gas under isothermal condition ($\Delta\varepsilon_T = \alpha\Delta T = 0$) can be written as:

$$\Delta\varepsilon_{axi} = \Delta\varepsilon_{e,axi} + \Delta\varepsilon_{ve,axi} + \Delta\varepsilon_{vp\text{-}st,axi} + \Delta\varepsilon_{vp\text{-}lt,axi} + \Delta\varepsilon^{s,axi} \tag{14}$$

In Eq. 14, $\Delta\varepsilon_{e,axi}$ represents axial elastic strain increment, $\Delta\varepsilon_{ve,axi}$ is axial visco-elastic increment, $\Delta\varepsilon_{vp\text{-}st,axi}$ and $\Delta\varepsilon_{vp\text{-}lt,axi}$ denote the visco-plastic creep increments in axial direction for the cases where short-term and long-term strengths of coal are exceeded by effective stress, respectively (see Eqs. 3 and 4). The elastic and consolidation strains induced by pore pressure depletion have competing effect with matrix shrinkage strain on coal permeability. Whereas matrix shrinkage strain results in an

increase in permeability, elastic and consolidation strains cause reduction in permeability. Creep can cause further reduction in permeability when gas desorption is terminated. Fig. 12 shows the experimental axial creep data and representative components of total axial strain under deviatoric loading and unloading conditions. Fig. 13 shows a typical deformation curve during gas desorption and after termination of gas desorption (creep only).

Fig. 14 shows the components of total axial strain namely elastic strain, consolidation and shrinkage strains, and creep for three effective stress increments. In Eq. 14, using Hooke's law, the axial elastic strain increment ($\Delta\varepsilon_{e,axi}$) due to change in effective stress can be written as:

$$\Delta\varepsilon_{e,\,axi} = \frac{1}{E_e}\left[\Delta\sigma_{eff,\,z} - \upsilon\left(\Delta\sigma_{eff,\,x} + \Delta\sigma_{eff,\,y}\right)\right] \tag{15}$$

where, υ can be obtained from axial and radial strain data and then, E_e can be obtained by rearranging Eq. 15.

Like creep, consolidation as a time-dependent deformation can be modelled using Eq. 10. Therefore, the following stress-strain equation can be used for modelling consolidation and shrinkage strains during gas desorption under isothermal condition:

$$\begin{aligned}\Delta\varepsilon_{axi}^{con,s} = {} & \frac{\Delta\sigma_{eff,z}}{E_{ve,z}}\left[1-\exp(-\frac{E_{ve,z}}{\eta_{ve,z}}t)\right] - \upsilon_{xz}\frac{\Delta\sigma_{eff,x}}{E_{ve,x}}\left[1-\exp(-\frac{E_{ve,x}}{\eta_{ve,x}}t)\right] \\ & -\upsilon_{yz}\frac{\Delta\sigma_{eff,y}}{E_{ve,y}}\left[1-\exp(-\frac{E_{ve,y}}{\eta_{ve,y}}t)\right] + \varepsilon_L\left(\frac{p}{p+P_L} - \frac{p_0}{p_0+P_L}\right)\end{aligned} \tag{16}$$

The values for unknown parameters of Eq. 16 can be obtained using the equation as regression and fitting it to the measured experimental strain data during desorption (consolidation and shrinkage strains), shown in Fig. 15. Also, the visco-elastic terms of Eq. 16 (first, second and third terms on the right side) can be used as regression to fit creep data in order to obtain the values for unknown parameters. Tables 1 and 2 present the mechanical properties of the coal sample for three effective stress increments and matrix shrinkage parameters after fitting the strain and the gas sorption data, respectively. It should be noted that it is assumed that the sample is isotropic in the elastic regime (i.e. $E_{e,x} = E_{e,y} = E_{e,z}$ and $\upsilon_{xz} = \upsilon_{zx} = \upsilon_{yz} = \upsilon_{zy} = \upsilon_{xy}$); For the inelastic regime, geomechanical properties in x and y directions are isotropic (i.e. $E_{ve,x} = E_{ve,y}$ and $\eta_{ve,x} = \eta_{ve,y}$).

The results show that at the beginning of gas desorption process, elastic behaviour has dominant effect on coal deformation. Shrinkage strain cannot be directly obtained due to unattainability of pore pressure. However, the consolidation and shrinkage strains induced by pressure depletion can be obtained by subtracting elastic strain from total strain. For the effective stress increment of $\Delta\sigma_{eff,axi} = 0.99\text{MPa}$, pore pressure equilibrium was reached at approximately 100 hrs when primary creep started to occur. For the other two effective stress increments of $\Delta\sigma_{eff,axi} = 1.48\text{MPa}$ and $\Delta\sigma_{eff,axi} = 1.91\text{MPa}$, pore pressure equilibrated at a longer time that caused relatively delayed creep process. The creep achieved under constant effective stress for the two latter cases is steady state. Primary creep may have been established during development of matrix shrinkage and consolidation strains. The elastic strain at the beginning of gas desorption can be attributed to instantaneous cleat compression and matrix shrinkage. However, it can be suggested that contribution of shrinkage strain to elastic deformation may be infinitesimal since shrinkage strain is a time-dependent and lengthy process, sometimes in order of months (Seidle and Huitt, 1995). The significant drop in permeability

over time can be associated with consolidation and creep in coal and dominant effect of cleat compression on coal permeability.

4. Model validation

To extend the application of the experimental findings, the permeabilty model introduced by Danesh et al. (2016) along with a permeability model developed for creep under constant effective stress were employed to validate their suitability by fitting the experimental coal permeability data. The validation aims to apply the permeability model to better predict CBM production performance.

The permeability model (Danesh et al., 2016) incorporating the impact of viscoelastic deformation (consolidation and shrinkage strains) on permeability of cleat and matrix assemblage is given below:

$$k = k_0 e^{-3c_f\left[\left(\frac{E_{e,x}E_{ve,x}}{E_{e,z}E_{ve,z}}\right)\left(\frac{\mathrm{E}_z}{\mathrm{E}_x}\right)\left(\frac{\nu_{zx}+\nu_{xy}\nu_{zy}}{1-\nu_{xy}^2}\right)(-\alpha\Delta P)-\frac{E_{e,x}E_{ve,x}\Delta\varepsilon_x^s}{(1-\nu_{xy})(\mathrm{E}_x)}\right]} \tag{17}$$

where,

$$\mathrm{E}_x = E_{ve,x} + E_{e,x}\left[1-\exp(-\frac{E_{ve,x}}{\eta_{ve,x}}t)\right] \tag{18}$$

$$\mathrm{E}_z = E_{ve,z} + E_{e,z}\left[1-\exp(-\frac{E_{ve,z}}{\eta_{ve,z}}t)\right] \tag{19}$$

Eq.17 is applicable under increased effective stress condition during methane desorption. Similar to the procedure carried out to develop the mentioned permeability model, the following permeability model that accounts for the impact of creep under constant effective stress is suggested as follows:

$$k = k_0 e^{-3c_f\left[\left(\frac{\nu_{zx}+\nu_{xy}\nu_{zy}}{1-\nu_{xy}^2}\right)(\Delta\sigma_{eff,z})-\frac{E_{ve,x}}{E_{ve,z}}\frac{\left[1-\exp(-\frac{E_{ve,z}}{\eta_{ve,z}}t)\right]}{\left[1-\exp(-\frac{E_{ve,y}}{\eta_{ve,y}}t)\right]}\right]} \tag{20}$$

where, $\Delta\sigma_{eff,z}$ is the axial effective stress generating creep in z direction at equilibrium, which can be calculated by incorporating experimental creep data in Hooke's law.

Eqs. 17 and 20 also show that fracture compressibility (C_f) is needed in order to determine coal permeability value. As can be seen, three different values have been used for calculation of fracture compressibility using Eq. 21. This is due to a relatively lengthy compaction process at each step of pore pressure depletion that results in significant alteration in fracture compressibility. Therefore, using a single value for fracture compressibility may result in higher deviation of numerical data from empirical data and hence higher uncertainty.

According to the definition, fracture compressibility can be calculated using the following equation:

$$C_f = \frac{-\ln\left(\frac{k}{k_0}\right)}{3\left(\sigma_h^e - \sigma_{h0}^e\right)} \tag{21}$$

where, ($\sigma_h^e - \sigma_{h0}^e$) is the change in horizontal effective stress. k is the permeability measured toward the end of creep process. k_0 is the initial permeability measured before the beginning of gas desorption process.

Table 3 presents the values for fracture compressibility for the three effective stress increments ($\Delta\sigma_{eff,axi}$).

Fig. 16 shows experimental measurements and values predicted using the permeability models (Eqs. 17 and 20). The mechanical properties of the coal sample used for the comparison between numerical results and experimental data are tabulated in Tables 1 and 2. It should be noted that it is assumed that the Poisson's ratios on zx, xy and zy plates, in the permeability models, are equal ($\upsilon_{zx} = \upsilon_{zy} = \upsilon_{xy}$). Also, it is assumed that $E_{e,x} = E_{e,z}$.

The permeability comparison made between empirical and numerical data shows a maximum deviation of approximately 15.4% at pore pressure of 0.5 MPa when $\Delta\sigma_{eff,axi} = 1.91$MPa (Fig. 17).

5. Conclusions

This study presented a series of experimental results for a coal sample saturated with helium first and then methane under triaxial condition. The impact of time-dependent deformation on coal permeability and gas production was investigated in detail. For the case of helium, the irrecoverable deformation and the loss of permeability due to creep are substantial. *RDR* of 14.1% was observed in this test. In addition, a significant *PLR* of 71% due to residual deformation was observed. The irrecoverable deformation may be due to the damage to coal microstructure resulted from granular creep and cataclasis. For the case of methane, the elastic strain triggered by gas desorption is caused by instantaneous cleat compression and matrix shrinkage. However, the contribution of cleat compression to elastic deformation is likely to be more significant than shrinkage strain as a relatively lengthy phenomenon. Removal of axial load resulted in an elastic strain recovery similar to the case of helium. This behaviour is due to instantaneous opening of cleats and expansion of matrix. The residual deformation may be resulted from consolidation, granular creep, and cataclasis; among which, consolidation can be recoverable to some extent. The extended stress-strain model was successful in matching creep strain curves. Similarly, the permeability model was successful in fitting the experimental permeability data. Mechanically induced compaction can cause temporary or permanent decrease in permeability during gas production depending on the dominant deformation mechanism. Contribution of consolidation and creep deformations, as partially recoverable mechanisms, to permeability reduction may constantly increase during gas production and well shut-in when pore pressure equilibrium is reached in consolidated zones in reservoir. In this study, a total reduction of 26% in permeability resulted from an increase of 1.91 MPa in effective stress due to methane desorption was observed. The permeability reduction can be linked to consolidation and creep strains in contrast to matrix shrinkage strain with increasing effects on coal permeability. This indicates that creep in coal, should be considered when evaluating and predicting reservoir performance. The experimental results of this study shed light on better understanding of complex interaction of gas transport and coal deformation.

Acknowledgements

The authors would like to acknowledge School of Mechanical and Mining Engineering of the University of Queensland for provision of the scholarship, the partial support by ARC Discovery

Project (DP150103467), and State Key Laboratory of Coal Resources and Safe Mining at China University of Mining and Technology (Project No.: SKLCRSM16KFA03). These sources of support are gratefully acknowledged. Furthermore, authors would like to acknowledge the contribution of CSIRO lab technicians, Mr David Down and Mr Michael Camilleri, to this paper and Dr Basil Beamish for provision of the coal sample.

References

Alexeev, A.D., Revva, V.N., Molodetski, A.V., 2012. Stress state effect on the mechanical behavior of coals under true triaxial compression conditions, in: Kwaśniewski, M., Li, X., Takahashi, M. (Eds.), True triaxial testing of rocks. CRC Press/Balkema, pp. 281-291.

Bai, Q., Xia, Y., Liu, X., Yang, Z., 2012. The study of the triaxial rheological test of the argillaceoussiltstone. Advanced Materials Research 446-449, 2125-2131.

Barden, L., 1968. Primary and secondary consolidation of clay and peat Geotechnique 18, 1-24.

Bjørlykke, K., Høeg, K., Mondol, N.H., 2010. Petroleum Geoscience: From Sedimentary Environments to Rock Physics. Springer, pp. 281-298.

Brantut, N., Heap, M.J., Meredith, P.G., Baud, P., 2013. Time-dependent cracking and brittle creep in crustal rocks: A review. Journal of Structural Geology 52, 17-43.

Cruden, D.M., Leung, K., Masoumzadeh, S., 1987. A technique for estimating the complete creep curve of a sub-bituminous coal under uniaxial compression. International Journal of Rock Mechanics and Mining Sciences 24, 265-269.

Danesh, N.N., Chen, Z., Aminossadati, S.M., Kizil, M.S., Pan, Z., Connell, L.D., 2016. Impact of creep on the evolution of coal permeability and gas drainage performance. Journal of Natural Gas Science and Engineering 33, 469-482.

Espinoza, D.N., Vandamme, M., Dangla, P., Pereira, J.M., Vidal-Gilbert, S., 2016. Adsorptive-mechanical properties of reconstituted granular coal: Experimental characterization and poromechanical modeling. International Journal of Coal Geology 162, 158-168.

Fabre, G., Pellet, F., 2006. Creep and time-dependent damage in argillaceous rocks. International Journal of Rock Mechanics and Mining Sciences 43, 950-960.

Fjær, E., Holt, R.M., Horsrud, P., Raaen, A.M., Risnes, R., 2008. Developments in Petroleum Science, Petroleum Related Rock Mechanics, 2nd ed. Elsevier, pp. 1-54.

Frayne, M.A., Mraz, D.Z., Rothenburg, L., 1990. A simple normalized isothermal constitutive law for modelling compaction creep behaviour of granular halite backfill. American Rock Mechanics Association.

Hobbs, D.W., 1964. The Strength and the Stress-Strain Characteristics of Coal in Triaxial Compression. Journal of Geology 72, 214-231.

Hol, S., Zoback, M.D., Spiers, C.J., 2013. Role of adsorption in the creep behavior of coal and shale Poromechanics V - Proceedings of the 5th Biot Conference on Poromechanics, pp. 668-677.

Jaeger, G.C., Cook, N.G.W., 1969. Fundamentals of Rock Mechanics. Chapman and Hall Ltd and Science Paperbacks, London.

Jaeger, J.C., Cook, N.G.W., Zimmerman, R.W., 2007. Fundamentals of Rock Mechanics. Blackwell Publishing, Malden.

Jiang, Q., Qi, Y., Wang, Z., Zhou, C., 2012. An extended Nishihara model for the description of three stages of sandstone creep. Geophysical Journal International 193, 841-854.

Kaiser, P.K., Morgenstein, N.R., 1981. Time-dependent deformation of small tunnels-I. Experimental facilities. International Journal of Rock Mechanics and Mining Sciences & Geomechanics 18, 129-140.

Levine, J.R., 1996. Model study of the influence of matrix shrinkage on absolute permeability of coal bed reservoirs. Geological Society, London, Special Publications 109, 197-212.

Li, Q., Xu, H., Bu, W., Zhao, G., 2011. An analytic solution describing the visco-elastic deformation of coal pillars in room and pillar mine. Mining Science and Technology (China) 21, 885–890.

Li, S., Qiang, Z., Chen, Z., 2013. Experimental study of compaction creep model of broken rock. Journal of Mining World Express 2, 76-81.

Lin, W., 2010. Gas sorption and the consequent volumetric and permeability change of coal, Department of Energy Resources Engineering. Stanford University, p. 195.

Liu, H.H., Rutqvist, J., 2010. A new coal-permeability model, internal swelling stress and fracture–matrix interaction. Transport in Porous Media 82, 157-171.

Nishihara, M., 1952. Creep of shale and sandy-shale. Journal of the Geological Society of Japan 58, 373-377.

Nishihara, M., 1957. Rheological properties of rocks. Doshisha Engng. Rev. 83, 85-115.

Palmer, I., Mansoori, J., 1996. How Permeability Depends on Stress and Pore Pressure in Coalbeds: A New Model. Society of Petroleum Engineers.

Palmer, I., Mansoori, J., 1998. How Permeability Depends on Stress and Pore Pressure in Coalbeds: A New Model, Annual Technical Conference & Exhibition. Society of Petroleum Engineers, Denver, pp. 539-544.

Pan, J., Meng, Z., Hou, Q., Ju, Y., Cao, Y., 2013. Coal strength and Young's modulus related to coal rank, compressional velocity and maceral composition. Journal of Structural Geology 54, 129-135.

Pan, Z., Connell, L.D., 2011. Modelling of anisotropic coal swelling and its impact on permeability behaviour for primary and enhanced coalbed methane recovery. International Journal of Coal Geology 85, 257-267.

Pan, Z., Connell, L.D., Camilleri, M., 2010. Laboratory characterisation of coal reservoir permeability for primary and enhanced coalbed methane recovery. International Journal of Coal Geology 82, 252-261.

Pomeroy, C.D., 1956. Creep in Coal at Room Temperature. Nature 178, 279-280.

Schatz, J.F., Carroll, M.M., 1981. Creep compaction of porous rock, Proceedings of the International Symposium on Weak Rock International Society for Rock Mechanics, Tokyo, Japan.

Seidle, J.P., Huitt, L.G., 1995. Experimental measurement of coal matrix shrinkage due to gas desorption and implications for cleat permeability increases, International Meeting on Petroleum Engineering. Society of Petroleum Engineers, Inc, Beijing, China, pp. 575-582.

Settari, A., 2002. Reservoir Compaction. Distinguished Author Series. Journal of Petroleum Technology 54, 62-69.

Shi, J.Q., Durucan, S., 2004. Drawdown induced changes in permeability of coalbeds: A new interpretation of the reservoir response to primary recovery. Transport in Porous Media 56, 1-16.

Singh, D.P., 1975. A Study of Creep of Rocks. International Journal of Rock Mechanics and Mining Sciences 12, 271-276.

Sone, H., Zoback, M.D., 2010. Strength, Creep And Frictional Properties of Gas Shale Reservoir Rocks. American Rock Mechanics Association.

Ujihira, M., Higuchi, K., Mizuma, H., 1985. On the Triaxial Compression Test of Coal and Other Specimens in Which High Pressure Gas is Involved, Hokkaido University, pp. 41-50.

Wang, D., Wei, J., Yin, G., Wang, Y., Wen, Z., 2011. Triaxial creep behavior of coal containing gas in laboratory. Procedia Engineering 26, 1001-1010.

Wang, J.G., Kabir, A., Liu, J., Chen, Z., 2012. Effects of non-Darcy flow on the performance of coal seam gas wells. International Journal of Coal Geology 93, 62-74.

Yang, Y., Zoback, M.D., 2011. The effects of gas adsorption on swelling, visco-plastic creep and permeability of sub-bituminous coal, Geomechanics Symposium held in San Francisco. American Rock Mechanics Association, CA.

Yin, G., Wang, D., Huang, G., Zhang, D., Wang, W., 2009. A triaxial creep model for coal containing gas and its stability analysis. Journal of Coal Science and Engineering 15, 248-251.

Yin, G., Wang, D., Zhang, D., Wei, Z., 2008. Research on triaxial creep properties and creep model of coal containing gas. Yanshilixue Yu Gongcheng Xuebao/Chinese Journal of Rock Mechanics and Engineering 27, 2631-2636.

Yost, F.G., Aronson, E.A., 1987. Crushed salt consolidation kinetics, Other Information: Portions of this document are illegible in microfiche products. Original copy available until stock is exhausted.

Zhu, J., Yang, X., He, N., 2011. Experimental Research on Coal Rock Creep Deformation-seepage Coupling Law, First International Symposium on Mine Safety Science and Engineering. Elsevier pp. 1526-1531.

Zhu, W., Wong, T.F., 1997. The transition from brittle faulting to cataclastic flow in porous sandstones: Permeability evolution. Journal of Geophysical Research 102, 3027-3042.

Figures

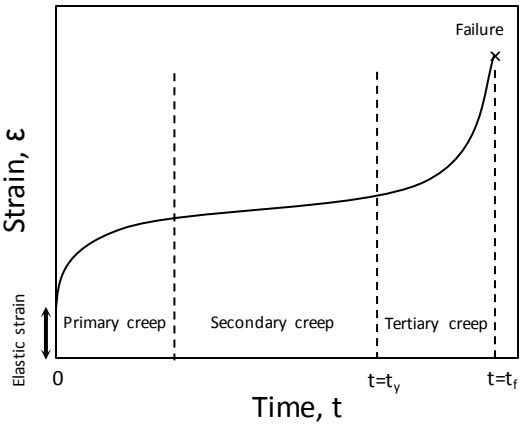

Fig. 1. Various stages of a typical creep curve under deviatoric stress (Yin et al., 2008)

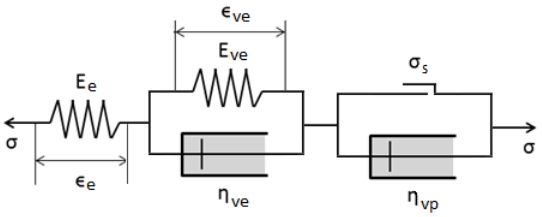

Fig. 2. Elements of classical Nishihara model (Nishihara, 1952)

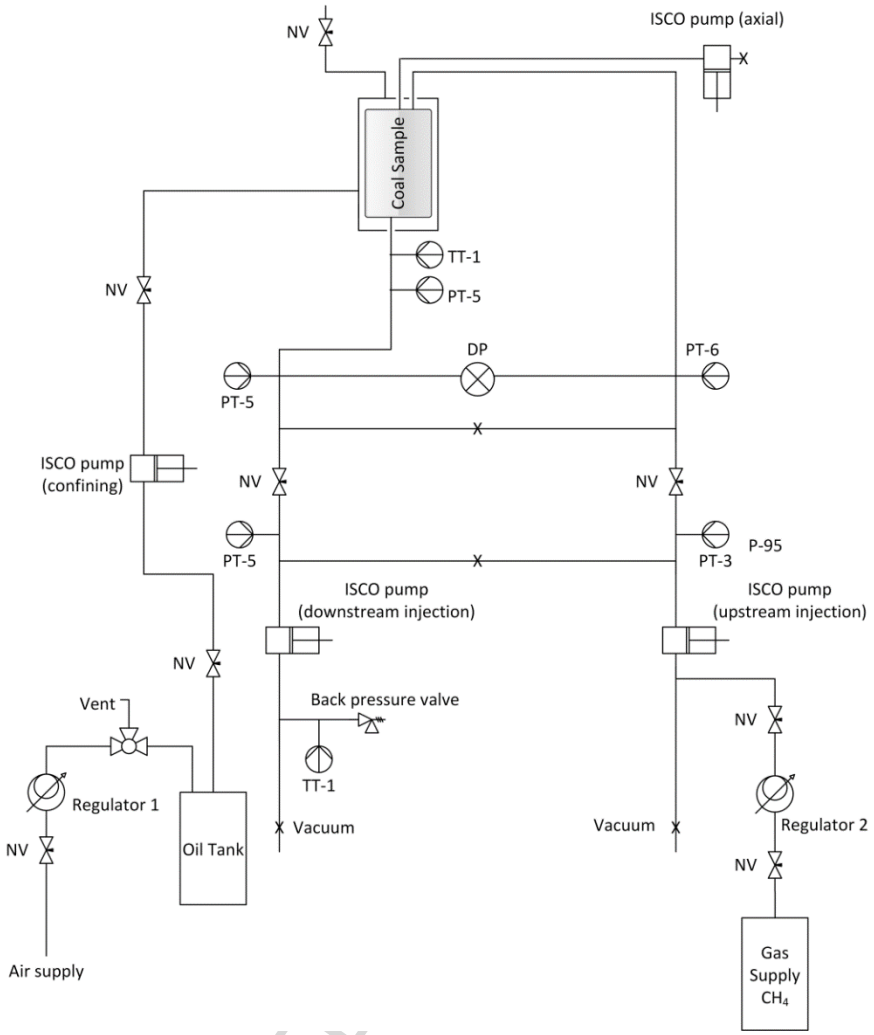

Fig. 3. Schematic of the triaxial gas rig

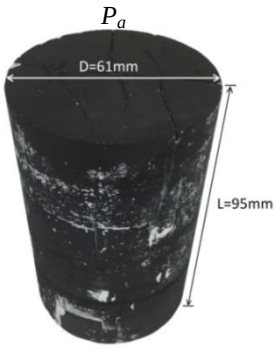

Fig. 4. Coal sample after preparation

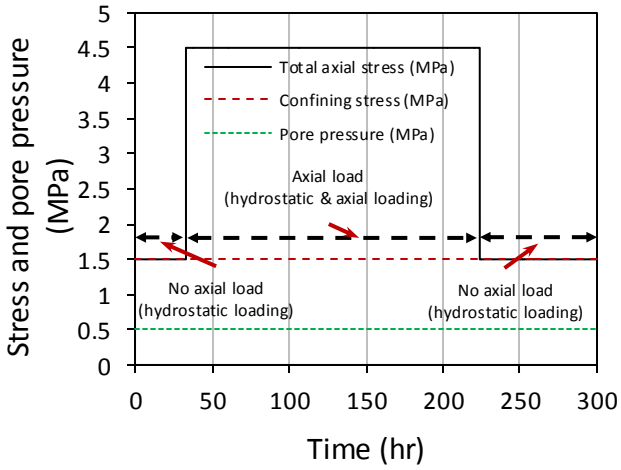

Fig. 5. Loading history and pore pressure of helium

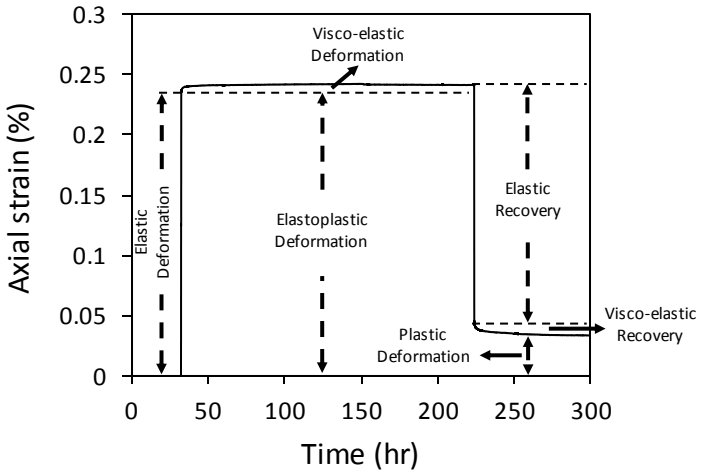

a)

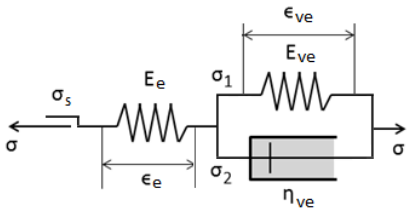

b)

Fig. 6. a) Experimental axial creep data and its components, b) rheological model

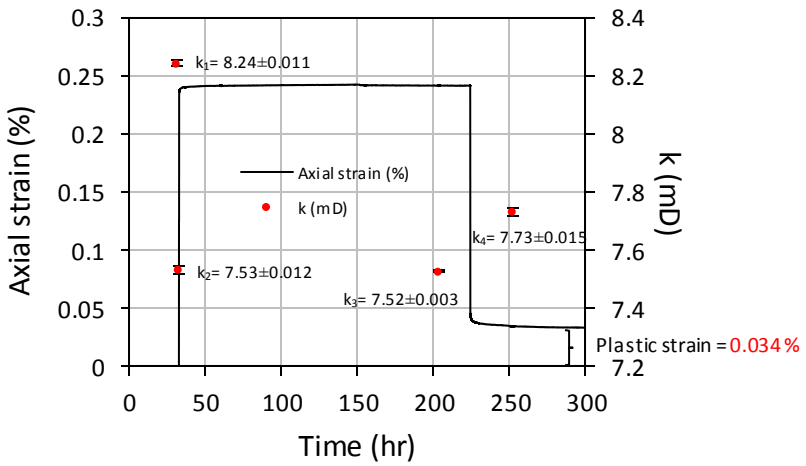

Fig. 7. Axial strain vs. time for helium under constant hydrostatic stress of 1.5 MPa when axial stress increased from 1.5 MPa to 4.5 MPa

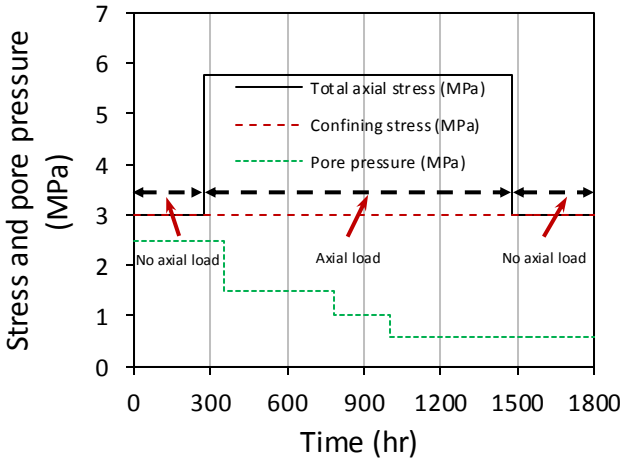

Fig. 8. Loading history and pore pressure of methane during gas desorption

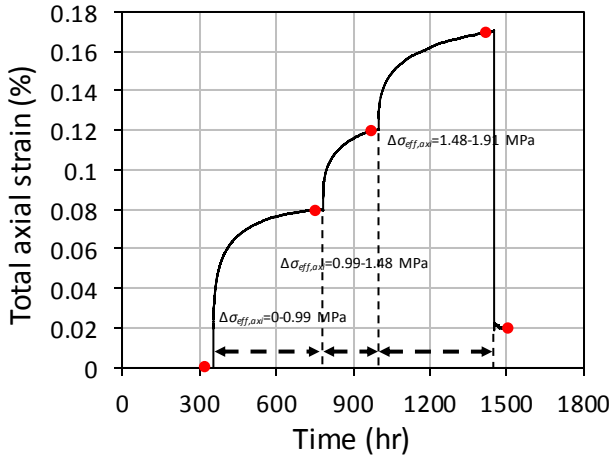

Fig. 9. Total axial strain vs. time for $\Delta\sigma_{eff,axi} = 0 - 0.99\text{MPa}$, $\Delta\sigma_{eff,axi} = 0.99 - 1.48\text{MPa}$, and $\Delta\sigma_{eff,axi} = 1.48 - 1.91\text{MPa}$

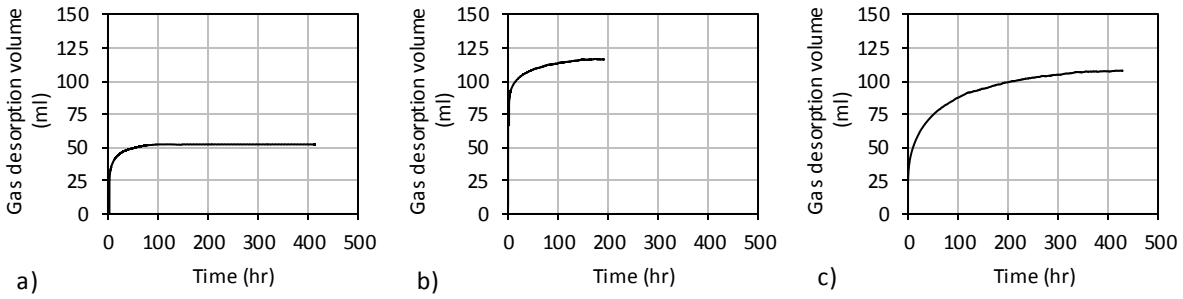

Fig. 10. Gas desorption volume vs. time at gas pressures of: a) 1.49 MPa, b) 1 MPa, and c) 0.57 MPa

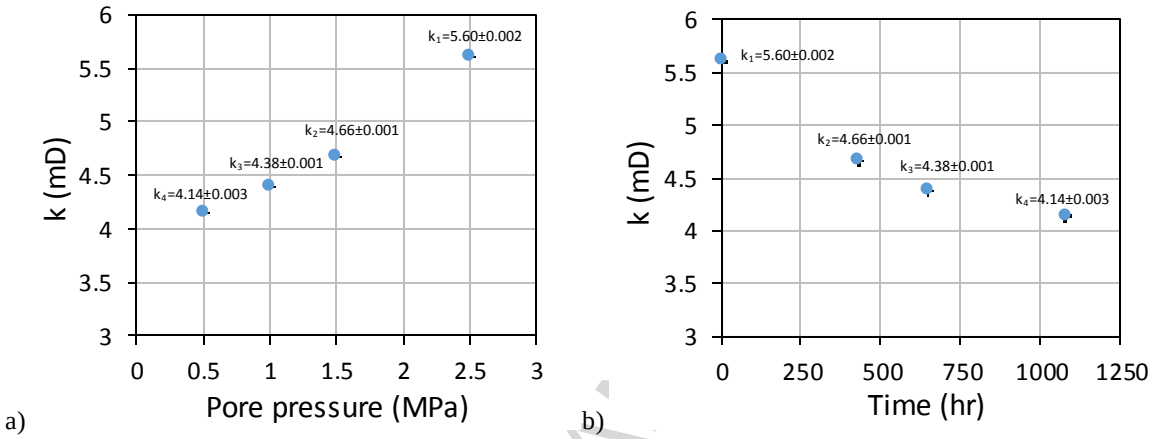

Fig. 11. Evolution of coal permeability: a) permeability vs. pore pressure, and b) permeability vs. time for $\Delta\sigma_{eff,axi} = 0 - 0.99\text{MPa}$, $\Delta\sigma_{eff,axi} = 0.99 - 1.48\text{MPa}$, and $\Delta\sigma_{eff,axi} = 1.48 - 1.91\text{MPa}$

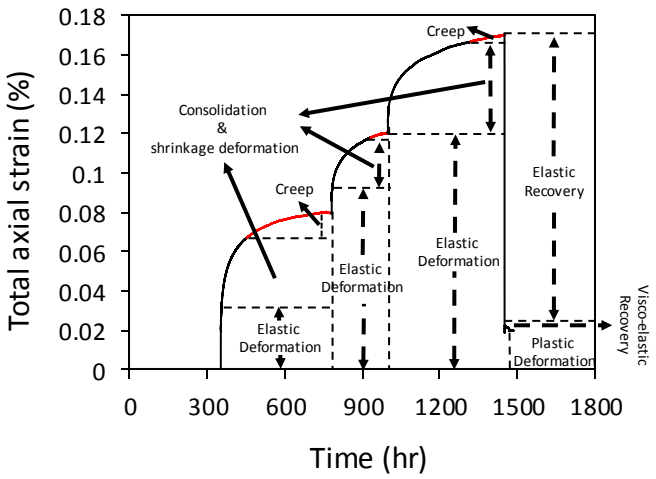

Fig. 12. Experimental axial creep data and its components

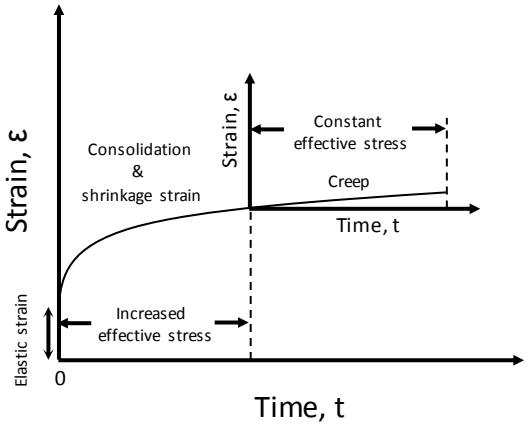

Fig. 13. A typical deformation curve during desorption (increased effective stress) and pore pressure equilibrium (constant effective stress)

a)

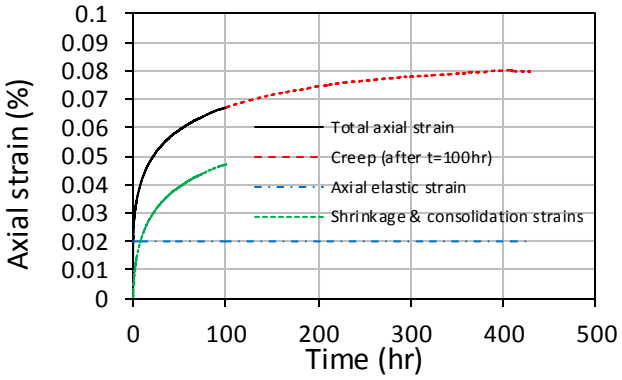

b)

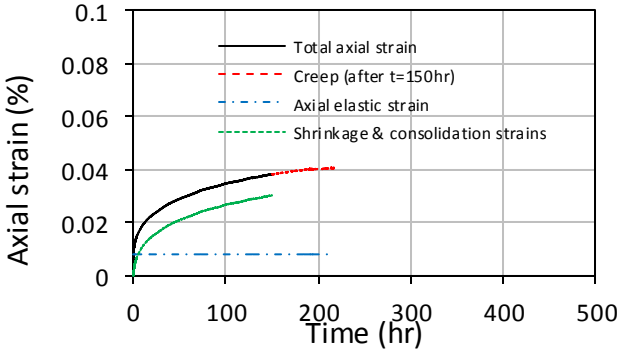

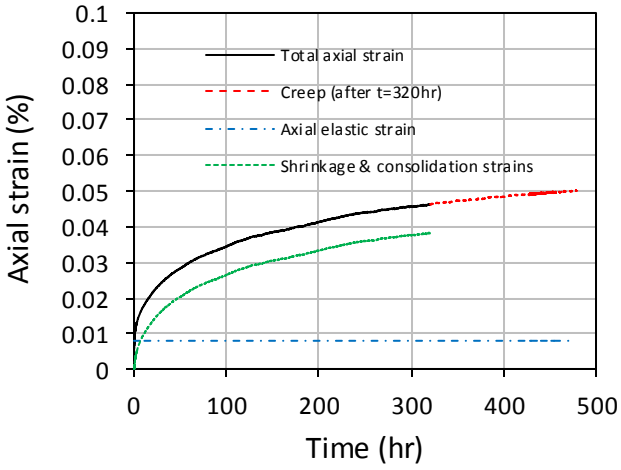

c)

Fig. 14. Axial strain components vs. time for a) $\Delta\sigma_{eff,axi} = 0 - 0.99\text{MPa}$, b) $\Delta\sigma_{eff,axi} = 0.99 - 1.48\text{MPa}$, and c) $\Delta\sigma_{eff,axi} = 1.48 - 1.91\text{MPa}$

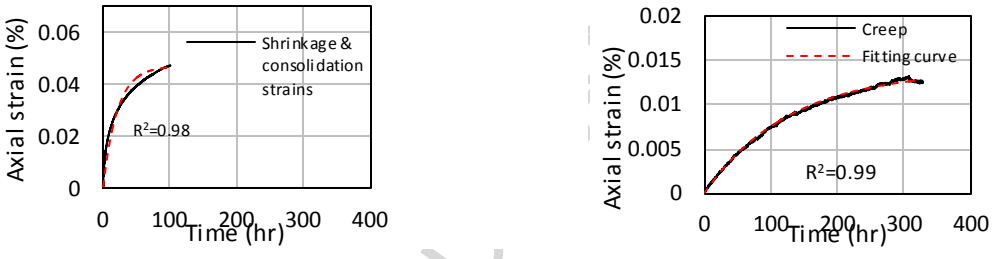

a)

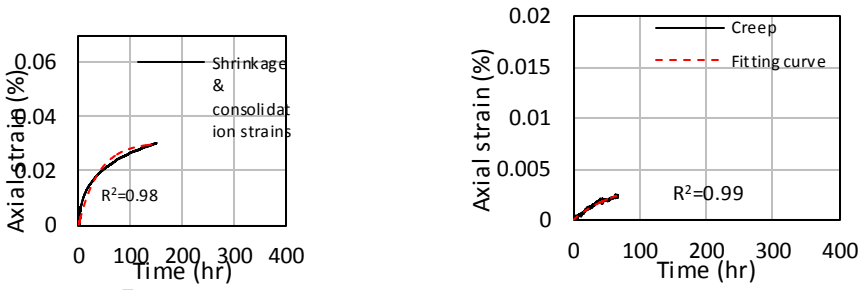

b)

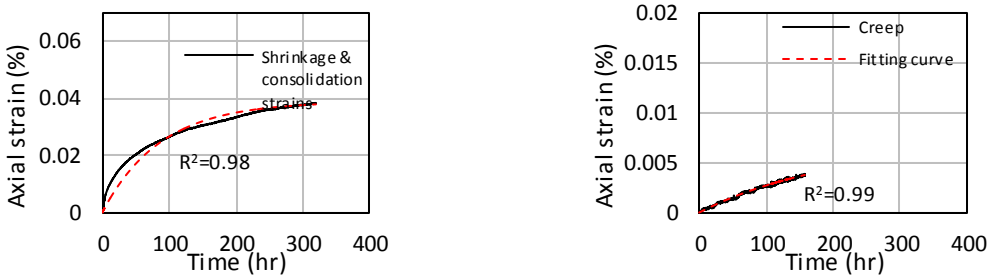

c)

Fig. 15. Curve-fitting measured strain data for a) $\Delta\sigma_{eff,axi} = 0 - 0.99\text{MPa}$, b) $\Delta\sigma_{eff,axi} = 0.99 - 1.48\text{MPa}$, and c) $\Delta\sigma_{eff,axi} = 1.48 - 1.91\text{MPa}$

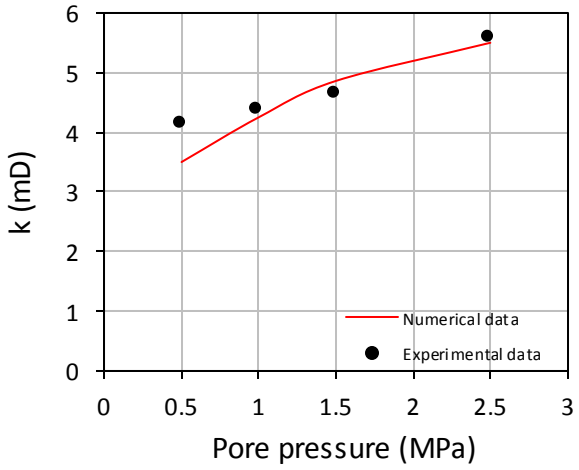

Fig. 16. Validation of permeability model

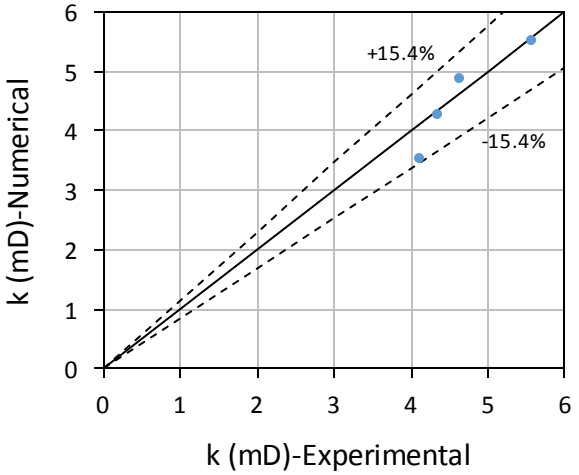

Fig. 17. Comparison of experimental and numerical permeability data

Tables

Table 1: Mechanical properties of the coal sample for three effective stress increments

Type of deformation	Mechanical properties	$\Delta\sigma_{eff,axi}$ (MPa)		
		[0-0.99]	[0.99-1.48]	[1.48-1.91]
Elastic strain	E_e (GPa)*	0.17	1.22	3.34
	ν*	0.48	0.44	0.30
Consolidation	$E_{ve,x}$= $E_{ve,y}$ (GPa)	1.90	4.60	8.00
	$E_{ve,z}$ (GPa)	0.85	1.95	4.47
	$\eta_{ve,z}$ (MPa.s)	6.54	27	140
	$\eta_{ve,x}$=$\eta_{ve,y}$ (MPa.s)	13.8	105	590
Creep	$E_{ve,x}$= $E_{ve,y}$ (GPa)	1.30	8.00	9.00
	$E_{ve,z}$ (GPa)	2.85	15.7	25
	$\eta_{ve,z}$ (MPa.s)	130	370	1800
	$\eta_{ve,x}$=$\eta_{ve,y}$ (MPa.s)	290	450	1650

Table 2: Matrix shrinkage parameters

V_L (m^3/kg)	0.02
P_L (MPa)	1.03
α (kg/m^3)	0.155
ε_L	0.0031

Table 3: Fracture compressibility for effective stress increments

$\Delta\sigma_{eff,axi}$ (MPa)	[0-0.99]	[0.99-1.48]	[1.48-1.91]
C_f (MPa^{-1})	0.061	0.040	0.037

Highlights

- A novel study on the impact of creep and residual deformation on coal permeability.
- The residual deformation can be due to the damage induced by creep mechanisms.
- Continuous drop in permeability due to consolidation and creep was observed.
- The previously developed model shows a good prediction of permeability.
- Considering the impact of creep on coal permeability is essential.